*J. Fluid Mech.* (2008), *vol.* 612, *pp.* 21–44.  
doi:10.1017/S0022112008002887 Printed in the United Kingdom

# Slender-body theory for steady sheared plumes in very viscous fluid

ROBERT J. WHITTAKER† AND JOHN R. LISTER

Institute of Theoretical Geophysics, Department of Applied Mathematics and Theoretical Physics, University of Cambridge, Wilberforce Road, Cambridge, CB3 0WA, UK

(Received 15 June 2007 and in revised form 15 May 2008)

A simple model based on slender-body theory is developed to describe the deflection of a steady plume by shear flow in very viscous fluid of the same viscosity. The key dimensionless parameters measuring the relative strengths of the shear, diffusion and source flux are identified, which allows a number of different dynamical regimes to be distinguished. The predictions of the model show good agreement with many, but not all, observations from previous experimental studies. Possible reasons for the discrepancies are discussed.

## 1. Introduction

Plumes arise from a localized and maintained source of buoyancy, possibly combined with a source of mass. They comprise a slender column of buoyant fluid rising (or falling) continuously under the influence of gravity (Turner 1973). Plumes are distinguished from episodic thermals, and from general convective overturning in equant convection cells, by being isolated and slender features. Any other motion in the surrounding fluid, which could be due to moving boundaries or to other scales of convection, affects the trajectory of a plume, causing it to be deflected or sheared from its natural vertical path.

Sheared plumes in very viscous fluid have a particular relevance to mantle convection. Persistent plumes originating within the mantle are thought to underlie hotspot tracks such as the Hawaiian–Emperor sea-mount chain. Wilson (1965) and Morgan (1971, 1972) comment on the variation in age of the volcanic rocks along the length of the tracks, which correlates roughly with the history of movement of the plates over the plumes. Detailed analysis shows that the relative motions of the inferred sources of such chains are typically much smaller than the observed plate motions (Molnar & Atwater 1973; Molnar & Stock 1987; Steinberger & O'Connell 1998), which suggests that the sources are much deeper in the mantle than the regions moving with the plates. Plumes are thus usually thought to originate from the thermal boundary layer above the core–mantle boundary, at a depth of about 3000 km. Jellinek & Manga (2002) and Davaille, Girard & Le Bars (2002), have recently suggested that the plume sources might then be anchored at nearly fixed positions on the core–mantle boundary by coupling of the thermal boundary layer with a thin compositionally dense layer (D″) at the base of the mantle. Whether this anchoring mechanism proves correct or not, the narrow plumes rising

† Present address: OCIAM, Mathematical Institute, University of Oxford, 24–29 St. Giles, Oxford, OX1 3LB.

through the mantle must penetrate and, to some extent, be deflected by the larger-scale convective overturning flow that is associated with sea-floor spreading and subduction.

Many authors have developed models for vertical rise in a mantle plume that is not significantly deflected by flow. These include early models of transport along a thermally induced low-viscosity conduit by Yuen & Schubert (1976) and Loper & Stacey (1983), which might be fed by steady drainage of a thermal boundary layer above the core–mantle boundary (Stacey & Loper 1983). These ideas were developed in calculations by Olson, Schubert & Anderson (1993) and Albers & Christensen (1996), among others, to model variations of the centreline temperature excess with height and buoyancy flux, for comparison with plume parameters observed at the top of the mantle. More recently, Steinberger (e.g. Steinberger & O'Connell 1998; Steinberger 2000) has made extensive efforts to relate detailed geophysical data from roughly 50 observed plumes to plume models and the effects of mantle motion. An excellent recent review of all this work from a geophysical perspective is given by Jellinek & Manga (2004); a review of fluid-mechanical models is provided by Whitehead (1988).

Plumes that rise through convection rolls in a quasi-steady manner will undoubtedly be deflected by the motion of the surrounding fluid. Sheared plumes have been studied experimentally, both with and without significant diffusion of the buoyancy (Skilbeck & Whitehead 1978; Whitehead 1982; Richards & Griffiths 1988, 1989). In these experiments, hot or compositionally buoyant fluid was introduced at the base of a cylindrical tank, with a rotating lid to generate a shear flow. Simple models were put forward to explain the observed behaviour and plume deflection. More recently, extensive diffusive experiments have been reported by Kerr & Mériaux (2004), who used a similar tank to generate a shear flow, but generated their plumes via a heating element set into the base.

The effects of shearing may also cause strongly tilted plumes to become unstable and break up into discrete blobs or diapirs. Experiments and theory on such breakup have been reported by Skilbeck & Whitehead (1978) and Whitehead (1982), who found plumes to become unstable when the angle $\theta$ to the vertical exceeds about 55°–60°. The authors discuss this instability as a possible mechanism for the chains of discrete islands in hotspot tracks. Related breakup experiments have also been performed by Olson & Singer (1985) though with a moving source in a stationary fluid, rather than a stationary source in a sheared fluid. The instability of a buoyant horizontal cylinder (i.e. the limit of $\theta \to 90°$) has been analysed theoretically by Lister & Kerr (1989), and linked to spatially episodic volcanism (Kerr & Lister 1988). However, as shown by experiments, a steady plume can be established without instability, provided the shear is sufficiently weak and the plume not deflected too far from the vertical.

Previous models of sheared plumes are somewhat unsatisfactory from a theoretical point of view, since they include free parameters that can be chosen to fit the data. Skilbeck & Whitehead (1978) applied slender-body theory to the plume, but assigned a constant value of $a/\ell = 0.1$ for the aspect ratio, rather than considering the correct external length scale to use. Richards & Griffiths (1988) proposed that the plume trajectory can be determined by adding a uniform vertical rise velocity to the horizontal advection by the background shear; this rise velocity is assumed to scale like the Stokes rise velocity of an isolated buoyant sphere of the same radius and buoyancy as the plume, but with an empirically determined multiplicative coefficient $k$ to account for the different (roughly cylindrical) geometry. This model predicts

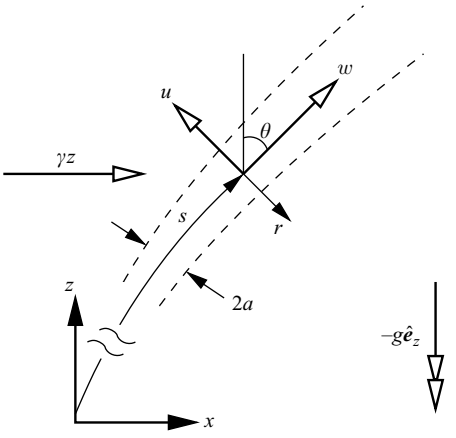


FIGURE 1. Definition sketch showing the coordinates and variables used to describe a sheared plume.

parabolic trajectories for the case of uniform shear and, after fitting the parameter $k$, yields remarkably good agreement with experiments.

In this paper we develop a model for steady sheared plumes that has no free parameters and has a more rigorous theoretical grounding than those proposed before. It should be noted that a simplifying assumption of our model is that the plume and ambient fluids have similar viscosities, which is often not the case in experiments or the mantle. Nevertheless, comparison with experiments suggests that the plume trajectory is insensitive to its viscosity and can be predicted as if it were the same as the ambient viscosity. The problem is formalized in § 2, and a model based on slender-body theory is developed in § 3, during which key dimensionless parameters are identified. The various possible dynamical regimes given by these parameters are discussed in § 4. We compare the model's predictions with the results of previous experiments in § 5, and provide some concluding remarks in § 6.

## 2. Problem description and governing equations

We consider a buoyant plume rising steadily through a uniform fluid of kinematic viscosity $\nu$ which is subject to an externally imposed uniform horizontal shear flow $\gamma z\hat{\boldsymbol{e}}_x$ (see figure 1). The external flow does not have to be a uniform shear and, as shown in § 5.3, the model can be used with other specified flows. However, uniform shear is convenient to realize experimentally, and is used in the theoretical development for definiteness and simplicity.

The additional velocity induced by the buoyancy in the plume is denoted by $\boldsymbol{u}$, the corresponding pressure perturbation by $p$, and the acceleration due to gravity by $-g\hat{\boldsymbol{e}}_z$. We assume that there is a rigid horizontal lower boundary at $z=0$, that the fluid is unbounded horizontally, and that it is either unbounded vertically or capped by a second horizontal boundary at $z=H$ (translating with velocity $\gamma H\hat{\boldsymbol{e}}_x$).

For the case of thermal buoyancy, we introduce the thermal diffusivity $\kappa$ and background temperature $T_0$. We assume that the equation of state can be linearized about $T_0$ over the range of temperatures under consideration and define the buoyancy field $b=g\beta(T-T_0)$, where $\beta=-\partial\ln\rho/\partial T|_{T_0}$ is the coefficient of thermal expansion. (For applications to the mantle, it would be necessary to use the potential temperature instead of temperature in order to account for adiabatic expansion.) We assume, for

simplicity, that inertia and any temperature dependence of the viscosity are both negligible. Applying the Boussinesq approximation, the governing equations are

$$\nu\nabla^2\boldsymbol{u} = \frac{1}{\rho_0}\nabla p - b\hat{\boldsymbol{e}}_z, \tag{2.1}$$

$$\nabla\cdot\boldsymbol{u} = 0, \tag{2.2}$$

$$(\boldsymbol{u} + \gamma z\hat{\boldsymbol{e}}_x)\cdot\nabla b = \kappa\nabla^2 b. \tag{2.3}$$

The boundary conditions are that $\boldsymbol{u}$, $p$ and $b$ decay in the far field, and that $\boldsymbol{u} = 0$ on the rigid boundaries. There are also some boundary conditions that describe the source at the base of the plume (see, for example, Whittaker & Lister 2006*a*,*b*). Since the model we develop here concerns only cross-sectionally averaged quantities, we require knowledge only of the initial mass flux $Q_0$ and buoyancy flux $B$ emitted by the source. It can be shown from (2.2) and (2.3) that $B$ is conserved along the length of a steady plume.

Equations (2.1)–(2.3) and their boundary conditions also apply to the case of compositional buoyancy provided $\kappa$ is replaced by the appropriate compositional diffusivity, possibly negligible, and $b$ is defined using the compositional difference $C - C_0$ between the plume and its environment and the compositional effect on density $-\partial\ln\rho/\partial C|_{C_0}$.

As shown in figure 1, we define an axial coordinate $s$ to measure the distance along the plume from its base, and local polar coordinates $(r, \phi)$ to describe the plane locally perpendicular to the plume axis (with $\phi = 0$ corresponding to the positive $x$ direction). The axial and transverse components of $\boldsymbol{u}$ in the $(x, z)$-plane are labelled $w$ and $u$ respectively; the third velocity component (in the $\hat{\boldsymbol{e}}_y$-direction) is labelled $v$, but is less important here.

## 3. Theoretical model

We aim to develop a simple leading-order model for the behaviour of a slender plume, that does not involve the detailed buoyancy distribution or velocity profile inside the plume. We describe the plume at each point $s$ along its axis by the inclination $\theta(s)$ from the vertical, the buoyancy per unit length

$$F(s) = \iint b\, r\, \mathrm{d}r\, \mathrm{d}\phi, \tag{3.1}$$

and a characteristic width $a(s)$, defined by

$$a^2 = \frac{1}{F}\iint b\, r^3\, \mathrm{d}r\, \mathrm{d}\phi. \tag{3.2}$$

We also define buoyancy-weighted average velocities

$$\overline{w}(s) = \frac{1}{F}\iint wb\, r\, \mathrm{d}r\, \mathrm{d}\phi, \tag{3.3}$$

$$\overline{u}(s) = \frac{1}{F}\iint ub\, r\, \mathrm{d}r\, \mathrm{d}\phi. \tag{3.4}$$

The corresponding mean velocity $\overline{v}$ perpendicular to the plane of the shear is zero by symmetry and does not appear in the model.

The model consists of equations that relate $\theta$, $F$, $a$, $\overline{u}$ and $\overline{w}$, and determines how they evolve along the length of the plume.

### 3.1. *Buoyancy fluxes and angle of inclination*

The diffusion of buoyancy in the axial direction is negligible compared to advection because the plume is assumed to be slender. The diffusion of buoyancy in the transverse direction may be significant, but has zero cross-sectional average. It follows that the total buoyancy flux $\boldsymbol{B}$ per unit length of the plume is dominated by the advective contribution. Hence

$$\boldsymbol{B} = \iint (\boldsymbol{u} + \gamma z \hat{\boldsymbol{e}}_x)\, b\, r \, \mathrm{d}r \, \mathrm{d}\phi = (\bar{\boldsymbol{u}} + \gamma z \hat{\boldsymbol{e}}_x)\, F. \tag{3.5}$$

In a steady state, the magnitude of the buoyancy flux is $B$ (the flux emitted by the source), and its direction defines the angle of inclination $\theta$ at each point along the plume. Taking the axial and transverse components of (3.5), see figure 1, we obtain

$$F = \frac{B}{\bar{w} + \gamma z \sin\theta}, \tag{3.6}$$

$$\bar{u} = \gamma z \cos\theta. \tag{3.7}$$

The axial component (3.6) relates the local buoyancy per unit length of plume to the conserved axial buoyancy flux $B$ and the total axial velocity $\bar{w} + \gamma z \sin\theta$. The transverse component (3.7) states that, since the buoyancy flux $\boldsymbol{B}$ is entirely axial in a steady state, the mean transverse velocity $\bar{u} - \gamma z \cos\theta$ must be zero.

### 3.2. *Slender-body theory*

The velocity field induced by the buoyancy in the plume can be described by slender-body theory (see Cox 1970; Batchelor 1970; Keller & Rubinow 1976; Hinch 1991, § 5.4). The basis of this theory is to use asymptotic methods to calculate an outer flow, which has a length scale $\ell$ much greater than the radius $a$ of the slender body, and to match it to an inner flow that has a length scale comparable to $a$. At leading order, the outer flow sees the plume as a curved line of zero thickness, which exerts a line force of axially varying strength $F(s)$. The inner flow sees the plume as a long straight cylinder of finite radius, within which there is a distributed body force $b(r, \phi)$ with negligible axial variation. The matching between the outer and inner flows is performed in the intermediate region $a \ll r \ll \ell$. Using standard results, we find that the outer flow driven by the plume is given in this region by

$$w \sim \frac{F\cos\theta}{2\pi\nu}\left\{-\ln\left(\frac{r}{\ell}\right) + C_1\right\}, \tag{3.8}$$

$$u \sim \frac{F\sin\theta}{4\pi\nu}\left\{-\ln\left(\frac{r}{\ell}\right) + \left(\cos^2\phi - \tfrac{1}{2}\right) + C_2\right\}, \tag{3.9}$$

where $F\cos\theta$ and $F\sin\theta$ are the local axial and transverse components of the buoyancy force per unit length. For $r \ll \ell$, the velocity is dominated by the logarithmic terms, which correspond to the logarithmic singularity of a line force in Stokes flow. (The term $\cos^2\phi - \frac{1}{2}$ is also part of the solution for a transverse line force, but is smaller than the logarithmic part.)

As discussed in Appendix A, the length scale $\ell$ of the external flow in (3.9) and (3.8) can be taken to be

$$\ell = \begin{cases} z & : \text{ no upper boundary} \\ z\left(1 - \dfrac{z}{H}\right) & : \text{ upper boundary at } z = H, \end{cases} \tag{3.10}$$

corresponding roughly to the distance to the nearest boundary.

The terms $C_i$ in (3.8) and (3.9) are $O(1)$ corrections to the leading-order approximation of the flow as that due to a straight uniform line force. In detail, they depend on the positions of the external boundaries, the complete curved shape of the plume, and the variation of $F(s)$ along the plume, but they are independent of the internal buoyancy distribution within the plume (which appears only at $O(a^2/r^2)$). In order to keep the model local, we approximate the $C_i$ by the expressions

$$C_1 = \ln 2 - 1 + \tfrac{1}{2}\sin^2\theta, \tag{3.11}$$

$$C_2 = \ln 2 - 2 + \sin^2\theta, \tag{3.12}$$

which depend only on the local value of $\theta$. As discussed in Appendix A, these approximations account for the local tilt $\theta$ of the plume and for the presence of the lower boundary, but not for the variations in $\theta$ and $F$ along the length of the plume. Since these variations appear to be relatively slow in the solutions of § 5, and since the $C_i$ are themselves only small corrections to the leading-order terms, we assume that the approximations (3.11) and (3.12) are satisfactory.

Since the interior flow must match to the inner limit of the outer flow, it must be almost the same as (3.8) and (3.9) evaluated at $r = a$. The mean velocities (3.3) and (3.4) are therefore written as

$$\overline{w} = \frac{F\cos\theta}{2\pi\nu}\left\{\ln\left(\frac{\ell}{a}\right) + C_1 + c_1\right\}, \tag{3.13}$$

$$\overline{u} = \frac{F\sin\theta}{4\pi\nu}\left\{\ln\left(\frac{\ell}{a}\right) + C_2 + c_2\right\}, \tag{3.14}$$

where the $c_i$ represent the deviation of the mean from the outer solution at $r = a$; they depend only on the local buoyancy distribution within the plume. The angular dependence on $\phi$ in (3.9) disappears in the averaging of (3.4).

In Appendix B we calculate the values of $c_1$ and $c_2$ for three representative buoyancy distributions. The values are found to be numerically small, and are not particularly sensitive to the actual distribution. For a top-hat profile we obtain $c_1 = c_2 = -0.097$ and for a Gaussian profile $c_1 = c_2 = -0.058$. Since $c_1$ and $c_2$ are much smaller than the leading-order logarithmic terms for $a/\ell \ll 1$ (and also smaller than the corrections $C_1$ and $C_2$), we shall use the fixed values $c_1 = c_2 = -0.1$. This avoids the need to calculate the buoyancy distribution within the plume.

### 3.3. *Diffusive growth*

Finally, we consider how the plume width $a$ varies due to the axial variation of velocity and the outward diffusion of buoyancy. In Whittaker & Lister (2006*b*), we defined the mass flux of a straight axisymmetric plume to be

$$Q(s) = \frac{2\displaystyle\int b\psi\,\mathrm{d}\psi}{\displaystyle\int b\,\mathrm{d}\psi}, \tag{3.15}$$

where $\psi$ is the streamfunction, and derived the exact result

$$Q(s) = Q_0 + 4\kappa s, \tag{3.16}$$

where $Q_0$ is the initial mass flux at the base of the plume. Thus, while the buoyancy flux $B$ is conserved, the mass flux $Q$ increases linearly along the plume owing to diffusion of buoyancy into the surrounding fluid. For a uniform axial flow $w_0(s)$,

$\psi = \frac{1}{2} w_0 r^2$ and it follows from (3.15) and (3.2) that $Q = a^2 w_0$, which establishes a relationship between the mass flux and the plume width. For a slender sheared plume, the flow is still approximately uniform on the scale of the plume width, and we can replace $w_0$ by the mean axial flow $\overline{w} + \gamma z \sin\theta$. We assume that the increase in the mass flux can then be approximated by (3.16), though a sheared plume is neither axisymmetric nor straight. We thus obtain

$$a^2 = \frac{4\kappa s + Q_0}{\overline{w} + \gamma z \sin\theta} \tag{3.17}$$

as a simple model of how stretching decreases and diffusion increases the plume radius.

This model neglects the possibility that $Q$ may increase owing to entrainment by the cross-stream circulation, as argued by Griffiths & Campbell (1991). This effect could be modelled by replacing (3.16) by $\mathrm{d}Q/\mathrm{d}s = c(\kappa a U)^{1/2}$, for some dimensionless constant $c$ and suitable velocity $U$, and replacing the numerator of (3.17) by $Q(s)$. The appropriate definition of $U$ is not obvious, but it may scale like $\bar{u}/\ln(\ell/a)$ since the circulation term in (3.9) is weaker than the logarithmic translational term. We note from (3.7) that $\bar{u}$ is itself small near the base of a plume or if the plume is weakly tilted. Moreover, we are principally concerned with the plume trajectory (rather than the precise evolution of $a$), and the trajectory depends only weakly on a logarithm of $a$. Hence, for simplicity, we will use (3.17) in our model.

### 3.4. *Non-dimensionalization*

From (3.6), (3.13) and (3.14), we scale velocities with $(B/2\pi\nu)^{1/2}$ and the buoyancy $F$ with $(2\pi\nu B)^{1/2}$. In order to obtain this velocity scale, the length and time scales $L$ and $T$ must be chosen such that

$$\frac{L}{T} = \left(\frac{B}{2\pi\nu}\right)^{1/2}. \tag{3.18}$$

As discussed below, there are a number of sensible choices for the length scale $L$ (and hence of $T$), the most convenient of which depends on the situation under consideration.

Rewriting (3.6), (3.7), (3.13), (3.14) and (3.17) in non-dimensional form, we obtain

$$\overline{w} = F\cos\theta \left\{ \ln\left(\frac{\ell}{a}\right) + C_1 + c_1 \right\}, \tag{3.19}$$

$$\bar{u} = \frac{F\sin\theta}{2} \left\{ \ln\left(\frac{\ell}{a}\right) + C_2 + c_1 \right\}, \tag{3.20}$$

$$\cos\theta = \frac{\bar{u}}{\mathscr{G} z}, \tag{3.21}$$

$$F = \frac{1}{\overline{w} + \mathscr{G} z \sin\theta}, \tag{3.22}$$

$$a^2 = \frac{\mathscr{K} s + \mathscr{Q}}{\overline{w} + \mathscr{G} z \sin\theta}, \tag{3.23}$$

where

$$\mathscr{G} = \gamma T, \qquad \mathscr{K} = \frac{4\kappa T}{L^2}, \qquad \mathscr{Q} = \frac{Q_0 T}{L^3}, \tag{3.24}$$

| Length scale $L$ | Time scale $T$ | Shear rate $\mathscr{G}=\gamma T$ | Diffusion $\mathscr{K}=\dfrac{4\kappa T}{L^2}$ | Mass flux $\mathscr{Q}=\dfrac{Q_0 T}{L^3}$ |
|---|---|---|---|---|
| $H$ | $H\left(\dfrac{2\pi\nu}{B}\right)^{1/2}$ | $\gamma H\left(\dfrac{2\pi\nu}{B}\right)^{1/2}$ | $\dfrac{4\kappa}{H}\left(\dfrac{2\pi\nu}{B}\right)^{1/2}$ | $\dfrac{Q_0}{H^2}\left(\dfrac{2\pi\nu}{B}\right)^{1/2}$ |
| $\left(\dfrac{B}{2\pi\nu\gamma^2}\right)^{1/2}$ | $\gamma^{-1}$ | 1 | $\dfrac{8\pi\nu\kappa\gamma}{B}$ | $Q_0\gamma^2\left(\dfrac{2\pi\nu}{B}\right)^{3/2}$ |
| $4\kappa\left(\dfrac{2\pi\nu}{B}\right)^{1/2}$ | $\dfrac{8\pi\nu\kappa}{B}$ | $\dfrac{8\pi\nu\kappa\gamma}{B}$ | 1 | $\dfrac{Q_0}{16\kappa^2}\left(\dfrac{B}{2\pi\nu}\right)^{1/4}$ |
| $Q_0^{1/2}\left(\dfrac{2\pi\nu}{B}\right)^{1/4}$ | $Q_0^{1/2}\left(\dfrac{2\pi\nu}{B}\right)^{3/4}$ | $\dfrac{4\kappa}{Q_0^{1/2}}\left(\dfrac{2\pi\nu}{B}\right)^{1/4}$ | $Q_0^{1/2}\gamma\left(\dfrac{2\pi\nu}{B}\right)^{3/4}$ | 1 |

TABLE 1. Examples of various choices of length scale $L$, along with the corresponding time scale $T$ and the resultant dimensionless parameters $\mathscr{G}$, $\mathscr{K}$ and $\mathscr{Q}$.

$\ell$, $C_1$ and $C_2$ are given by (3.10)–(3.12), and $c_1=c_2=-0.1$. These equations form the plume model.

The dimensionless parameters $\mathscr{G}$, $\mathscr{K}$ and $\mathscr{Q}$ can be viewed as non-dimensional forms of the shear rate, thermal diffusivity, and initial mass flux respectively. Their values depend on the fluid and source properties, the applied shear rate, and the chosen length and time scales.

The choice of $L$ can be adapted to the situation under consideration. When an upper boundary is present at $z=H$ and the plume behaviour over the full range of $z$ is of interest, then it is probably most sensible to set $L=H$ so that the dimensionless height of the ambient flow becomes unity. If the upper boundary is remote then, depending on what behaviour is of interest and which experimental parameters are being changed, it may be more convenient to choose the length scale $L$ so that one of $\mathscr{G}$, $\mathscr{K}$ or $\mathscr{Q}$ is unity. For example, choosing $L$ so that $\mathscr{G}=1$ has the effect that shear becomes important over an $O(1)$ dimensionless height (see § 4). Various scalings and the resulting values of the three dimensionless parameters are shown in table 1.

## 4. Transition heights and parameter regimes

There are several places in (3.19)–(3.23) where two terms are added together, raising the possibility that one term or other will dominate in some region of the plume. The change-overs between such regions of dominance lead to three (non-dimensional) transition heights:

(i) The height $h_a$ at which the plume starts to become slender, given by $\ell/a=O(1)$. This is where the logarithmic terms in (3.19) and (3.20) start to dominate the constant terms.

(ii) The height $h_d$ at which outward diffusion starts to have a significant effect on the width of the plume, given by $\mathscr{K}s\sim\mathscr{Q}$. This is where the two terms in the numerator of (3.23) balance.

(iii) The height $h_s$ at which the background shear velocity becomes comparable to the rise velocity of plume, given by $\overline{w}\sim\mathscr{G}z$. This is where the terms in the denominators of (3.22) and (3.23) become comparable.

We only consider the case $h_a\ll h_s$ in which the plume becomes slender before it suffers significant shearing. We make this restriction so that slender-body theory, and

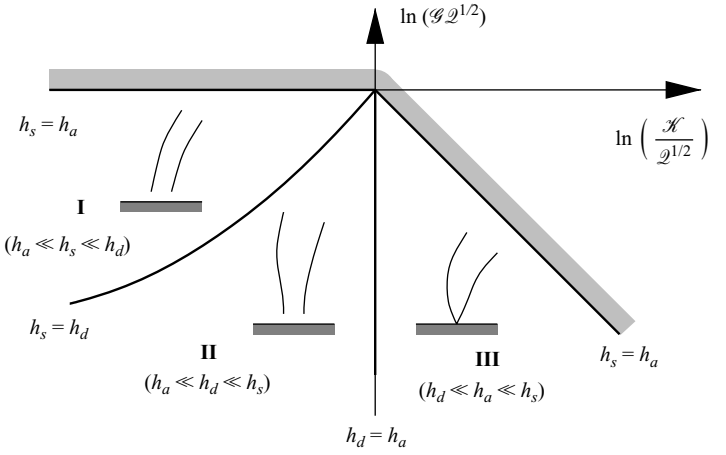


FIGURE 2. A regime diagram for sheared plumes, based on the three dimensionless parameters $\mathscr{G}$, $\mathscr{K}$ and $\mathscr{Q}$, as defined in (3.24). The upper-right region corresponds buoyant regions that would suffer significant shearing before they become slender plumes, which we do not consider here. The three labelled regimes correspond to different orderings of the transition heights (4.1)–(4.3).

hence the model, is applicable in the region in which the plume is being sheared. (In the opposite case, shear advects the buoyant fluid away from the source before it is able to rise and form a slender plume.)

We now use scaling arguments to examine how the transition heights are related to the dimensionless parameters $\mathscr{G}$, $\mathscr{K}$ and $\mathscr{Q}$. We first consider the case where the fluid domain is sufficiently high that $\ell = z$ is a good approximation at each of the transition heights. We note that for $z \lesssim h_s$, the angle of inclination is not yet close to horizontal, so that $\cos\theta = O(1)$, $\overline{w} \gtrsim \mathscr{G} z \sin\theta$ and $s \sim z$.

The plume becomes slender when $z \sim h_a \ll h_s$. By definition, $\ell/a = O(1)$ there, and by examining (3.19) and (3.22) we find that $\overline{w} \sim F \sim 1$. Then (3.23) implies

$$h_a \sim \max\{\mathscr{Q}^{1/2}, \mathscr{K}\}. \tag{4.1}$$

We can only evaluate the diffusion height $h_d$ when it satisfies $h_d \lesssim h_s$. In this case, $s \sim z$, and $\mathscr{K} s \sim \mathscr{Q}$ implies that

$$h_d \sim \frac{\mathscr{Q}}{\mathscr{K}}. \tag{4.2}$$

When $h_d \gg h_s$, the arclength $s$ could be significantly larger than the height $z$, and we are unable to relate the two without solving the model in detail.

Finally, for the shear height $h_s$, we first estimate $\overline{w} \sim (\ln(\ell/a))^{1/2}$ using (3.19) and (3.22). Then $\overline{w} \sim \mathscr{G} h_s$ implies that

$$h_s \left[\ln\left(\frac{h_s}{a(h_s)}\right)\right]^{-1/2} \sim \frac{1}{\mathscr{G}}. \tag{4.3}$$

The width $a(h_s)$ may be estimated from (3.23) using $s \sim h_s$ and the estimate of $\overline{w}$.

With the restriction $h_a \ll h_s$, there are three possible orderings of the transition heights, which lead to three different dynamical regimes, as shown in figure 2:

Plumes in Regime I ($h_a \ll h_s \ll h_d$) suffer significant deflection before they start to thicken diffusively. This obviously includes the non-diffusive case of immiscible fluids.

Plumes in Regime II ($h_a \ll h_d \ll h_s$) have the diffusive and shear heights reversed, so now the plume thickens diffusively before it suffers a significant deflection. However, since $h_a \ll h_d$, there is still a lower region where the plume is slender but behaves in a non-diffusive manner (cf. $z \ll z^*$ in Whittaker & Lister 2006*b*). Such plumes must originate from a distributed source.

Plumes in Regime III ($h_d \ll h_a \ll h_s$) appear the same as those in regime II at the $O(h_s)$ heights where shearing takes place. But lower down, there is no slender non-diffusive behaviour; the plume is already behaving diffusively when it becomes slender. Such plumes originate from a point source (cf. Whittaker & Lister 2006*a*).

Each point on the regime diagram (figure 2) corresponds to a single plume. However the characteristics of the plume may change along its length, as $z$ passes through each of the transition heights. Thus the plume corresponding to a specific point in parameter space may appear to have different characteristics depending on the height scale over which it is viewed. For example, in Regime II a plume first rises nearly vertically with constant mass flux, then starts to grow diffusively, and then becomes bent over by the shear.

Consider now how the results above are affected by the presence of a rigid boundary at $z = H$, when $H$ is not significantly larger than all of the transition heights. Clearly, we should ensure that $h_a \ll H$ so that the plume is slender over most of the domain, and that $h_s \lesssim H$ so that there is some shearing to be observed. With the presence of an upper boundary, the length scale $\ell$ is smaller at each height than in unbounded fluid (see (3.10)), and hence $h_a$ will be larger. There will also be a region adjacent to the upper boundary where $a/\ell \gtrsim O(1)$ and the plume is not slender. Vertical motion will be inhibited by the boundary, so the plume will be deflected more (hence $h_s$ will be reduced) and will appear to widen more rapidly by outward diffusion (hence $h_d$ will be reduced). Away from the upper boundary, the length scale $\ell$ and the induced velocities will have the same order of magnitude as they would in the absence of the boundary. Therefore, the behaviour away from the upper boundary will be qualitatively similar.

Numerical calculations for mantle plumes (e.g. Albers & Christensen 1996; Steinberger & O'Connell 1998) suggest that they span Regimes I and II, since both shear and diffusion can have significant effects over the 3000 km vertical scale of the mantle. It should be noted that the buoyancy fluxes of observed plumes vary by more than an order of magnitude, as may the horizontal shear rate at different depths in the mantle.

## 5. Comparison with experiments

Relevant experimental results have been reported by Richards & Griffiths (1988) and Kerr & Mériaux (2004). In both cases the authors generated a low-Reynolds-number shear flow in a vertically orientated cylindrical tank by rotating a circular lid in contact with the fluid. A buoyant plume was released from an off-centre position on the base, and observed as it rose through the sheared fluid. From the reported experimental parameters, we calculated the corresponding values of $\mathscr{G}$, $\mathscr{K}$ and $\mathscr{Q}$ using the fluid depth $H$ as the length scale $L$.

We then applied the model developed above to solve for the trajectory of a sheared plume using a simple numerical marching scheme that integrates up from the source. We started a little way above $z = 0$, since the plume needs to be sufficiently slender for (3.19) and (3.20) to give reasonable estimates of the velocity. In practice, $z_{\min} = 5h_a$,

| No. | $\mathscr{G}w^*$ | $\mathscr{K}$ | $\mathscr{Q}/w^*$ | $w^*$ | $\mu_i/\mu_0$ |
|---|---|---|---|---|---|
| A1 | 3.98 | 0 | $0.32 \times 10^{-4}$ | 1.88 | 0.07 |
| A2 | 0.996 | 0 | $1.28 \times 10^{-4}$ | 1.69 | 0.07 |
| A3 | 0.283 | 0 | $4.50 \times 10^{-4}$ | 1.49 | 0.07 |
| B1 | 1.73 | 0 | $1.60 \times 10^{-4}$ | 1.65 | 0.25 |
| B2 | 0.661 | 0 | $4.19 \times 10^{-4}$ | 1.47 | 0.25 |
| B3 | 0.290 | 0 | $9.54 \times 10^{-4}$ | 1.35 | 0.25 |

TABLE 2. Values of the dimensionless parameters inferred from the experiments of Richards & Griffiths (1988) based on the outer viscosity $\mu_0$. The factor $w^*$ is defined by (5.1) and is used to infer $B$ and $Q_0$ from the plume diameter. The groups $\mathscr{G}w^*$ and $Q/w^*$ are independent of $w^*$ and are calculated directly from the reported parameters. The viscosity ratio $\mu_i/\mu_0$ is of the plume to the ambient fluid.

as defined by (4.1), was found to be a suitable starting point at which $\ln(\ell/a)$ was large enough to ensure that $w, u > 0$.

Since the model is local, the only parameters required for a non-zero start are the initial horizontal displacement and trajectory length. In the comparisons shown here, we obtain the horizontal displacement by aligning the experimental plume and the corresponding prediction at $z = 5h_a$ and we assume that $s = z$ at $z = 5h_a$. This assumption is a good approximation provided the initial deflection is not too large, which will certainly be the case if $h_a \ll h_s$. The initial value of $s$ is only needed for the mass flux factor $\mathscr{K}s + \mathscr{Q}$ in (3.23) and thus only affects diffusing plumes for which $\mathscr{K} \neq 0$. Even with diffusion, a small error in $s$ only enters the rest of the model through a weak logarithmic factor, and so is not likely to have a significant effect on the trajectory.

### 5.1. *Richards & Griffiths (1988)*

Richards & Griffiths used glycerol as the ambient fluid, in a tank of radius $R = 30\,\text{cm}$ with a fluid depth $H = 9.5$ or $10.5\,\text{cm}$. A compositionally buoyant plume (of a glycerol and water mixture) was released through a hole in the bottom of the tank at a distance $R_p = 12\,\text{cm}$ from the axis. Molecular diffusion was negligible over the time scales involved. The rotation rate of the lid, and the properties of the injected fluid were varied between different runs. The injected fluid was 4 or 15 times less viscous than the ambient fluid.

Unfortunately Richards & Griffiths did not report the injection velocity or initial mass flux, so we could not calculate $Q_0$ and $B$ directly. One constraint follows from the reported values of the density difference $\Delta\rho = B/gQ_0$ between the plume and the ambient fluid. A second constraint is provided by the observed diameter $d$ of the plume, which was used as follows. Let $w^*$, a dimensionless axial velocity, be defined such that

$$Q_0 = \pi \left(\frac{d}{2}\right)^2 \left(\frac{B}{2\pi\nu}\right)^{1/2} w^*. \tag{5.1}$$

Both $B$ and $Q_0$ can then be expressed in terms of $w^*$ and known experimental parameters. Finally, the velocity $w^*$ was chosen so that the model predicted a plume of the observed diameter.

The dimensionless parameters corresponding to the experiments reported are shown in table 2. The shear rate $\gamma$ was calculated by assuming that the velocity varied linearly in $z$ between the stationary base and moving lid directly above the source. Since the

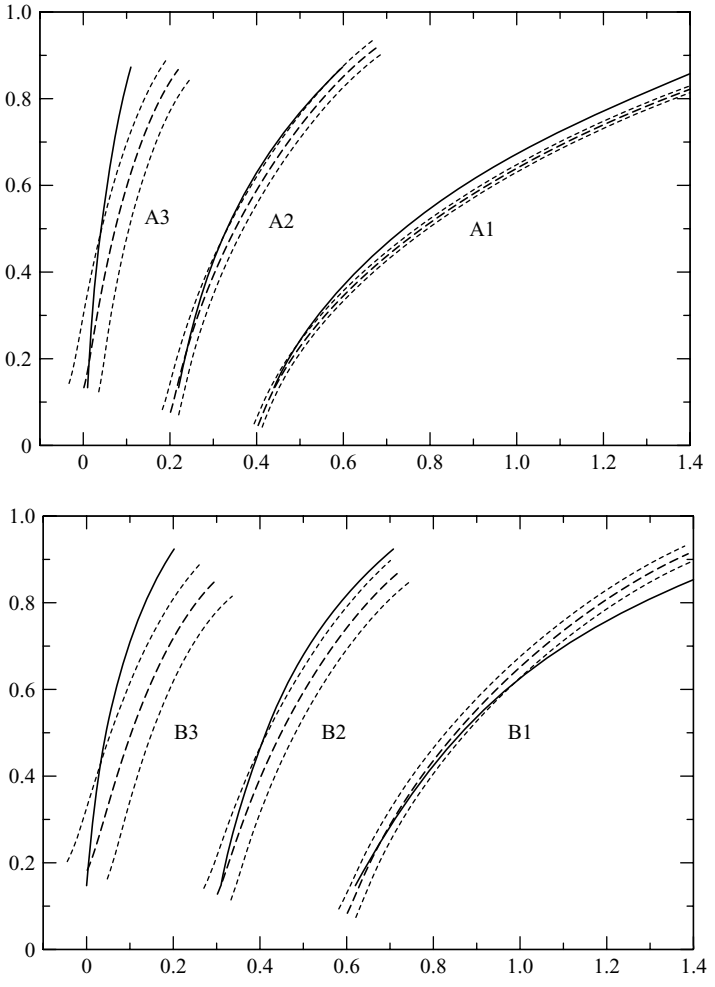


FIGURE 3. Comparison of the model predictions (dashed lines) with the experimental observations (solid lines) of Richards & Griffiths (1988). The predicted plume edges are at $\pm\sqrt{2}\,a$ corresponding to the top-hat buoyancy profile of a non-diffusing plume. The horizontal and vertical coordinates are non-dimensionalized by the height $H$ of the domain. Arbitrary horizontal off-sets have been introduced to separate the different experiments.

plumes are essentially non-diffusing, $\mathscr{K} = 0$ and the experiments lie in Regime I of figure 2. Non-dimensionalizing by the tank height $H$, we have $h_a = O(10^{-2})$, $h_d = \infty$ and $h_s = O(1)$.

The results from the model are compared with the experiments in figure 3. The agreement is fairly good, except at the two lower (dimensionless) shear rates (A3 and B3), for which the plumes are not particularly slender.

### 5.2. *Kerr & Mériaux (2004)*

Kerr & Mériaux studied diffusing thermal plumes in both glycerol and glucose syrup. Their tank had radius $R = 30\,\text{cm}$ and height $H = 24\,\text{cm}$ (except for one experiment done with $H = 12\,\text{cm}$). The plumes were generated by a heated disk at the lower boundary, a distance $R_\text{p} = 15\,\text{cm}$ from the axis. They were visualized using a pair of injected dye streams (assumed to act as passive tracers). The heating power, fluid

| No. | $\mathscr{G}$ | $\mathscr{K}/10^{-4}$ | $\mathscr{Q}/10^{-4}$ | $\mu_{\mathrm{i}}/\mu_0$ |
|---|---|---|---|---|
| 6 | 0.425 | 7.61 | 4.44 | 0.32 |
| 8 | 1.03 | 7.61 | 4.44 | 0.32 |
| 12 | 0.175 | 3.80 | 2.80 | 0.090 |
| 14 | 0.425 | 3.80 | 2.80 | 0.090 |
| 18 | 0.425 | 7.77 | 4.50 | 0.087 |
| 20 | 1.03 | 7.77 | 4.50 | 0.087 |

TABLE 3. Values of the dimensionless parameters inferred from the experiments of Kerr & Mériaux (2004), based on the outer viscosity $\mu_0$. The ratio with the viscosity $\mu_{\mathrm{i}}$ of the hottest fluid in the plume is also shown.

properties and lid rotation rate were all varied to investigate their effects on the plumes.

It is not obvious how to measure the initial mass flux $Q_0$ in the experiments, and understandably Kerr & Mériaux did not attempt to do so. Nevertheless, a value of $Q_0$ is required in our model. This was computed by using the quoted flux Rayleigh number $Ra_Q$ (defined in terms of the power consumption of the heating element) and results from Whittaker & Lister (2006*b*) for the boundary layer above a heated disk.

Whittaker & Lister derived the following expressions for the mass flux $Q_0$ and Nusselt number $Nu$, in terms of a Rayleigh number $Ra$ based on the radius $a_{\mathrm{s}}$ of the source:

$$Q_0 \sim 0.956\,\kappa a_{\mathrm{s}}\, Ra^{1/5}, \tag{5.2}$$

$$Nu \sim 2.90\, Ra^{1/5}. \tag{5.3}$$

The flux Rayleigh number defined by Kerr & Mériaux (2004) is related to these quantities by $\pi Ra_Q = Nu\, Ra$. Eliminating $Nu$ and $Ra$, we therefore obtain

$$Q_0 = 0.969\,\kappa a_{\mathrm{s}}\,(Ra_Q)^{1/6}. \tag{5.4}$$

It should be noted that the results of Whittaker & Lister (2006*b*) apply only to an isoviscous fluid, whereas the experiments of Kerr & Mériaux have significant viscosity variations (see table 3). However, a global change in viscosity would enter only though the factor of $Ra$, and hence errors in $Q_0$ are bounded by a factor of the viscosity ratio to the 1/6th power in (5.4). Furthermore, $Q_0$ only affects the plume trajectory via the weak logarithmic dependence on $a$, so neglect of the viscosity variations should not have a significant effect on the results present here.

Initially, we follow Kerr & Mériaux (2004) and assume that the shear rate $\gamma$ experienced by the plume was uniform in $z$. The dimensionless parameters corresponding to six experiments are shown in table 3. The similar values of $\mathscr{K}$ and $\mathscr{Q}$ suggest that $h_d$ is comparable to $H$. Since $\mathscr{G} = O(1)$ and the aspect ratios of the plumes are not particularly large, $h_s$ is also comparable to $H$. Therefore the experiments are roughly on the border $h_s \sim h_d$ between Regimes I and II of figure 2.

The results from the model are compared with the experiments in figure 4. There is very poor agreement, except in the qualitative trends, and it would appear that the shear velocity experienced by the experimental plumes is much less than that estimated, as done above, by assuming uniform shear between the moving lid and stationary source.

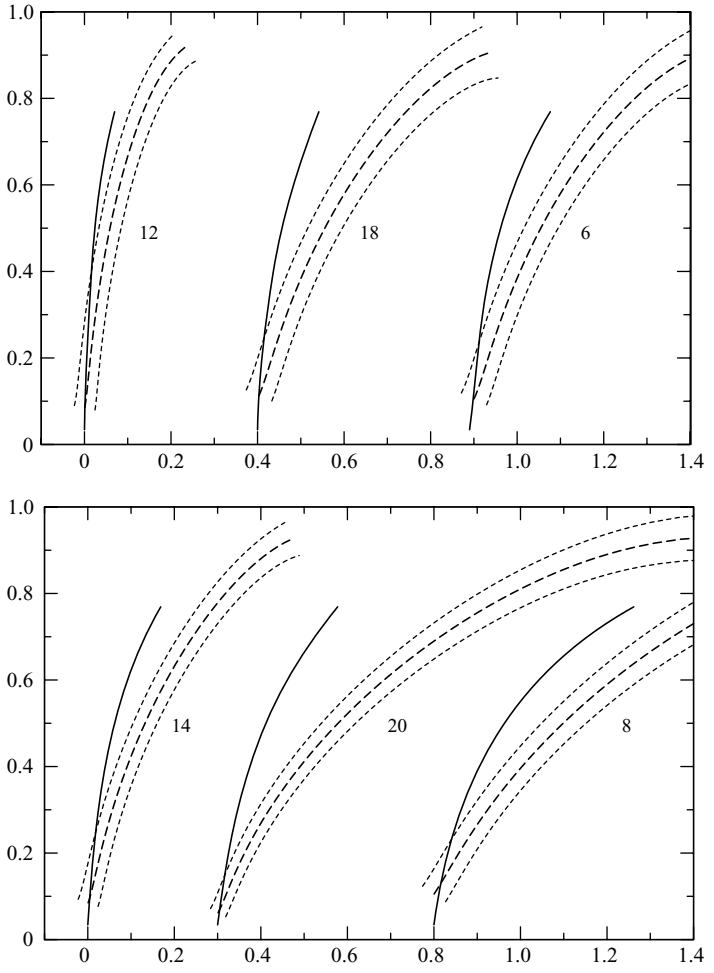


FIGURE 4. A comparison of the model predictions (dashed) assuming a uniform shear velocity with the experiments of Kerr & Mériaux (2004) (solid). The plume edges, though somewhat arbitrary for a diffusing plume, are shown at $\pm\sqrt{2}a$ for comparability with figure 3. The poor agreement in deflection is because the shear in the experiments was not actually uniform.

### 5.3. *Calculations with non-uniform shear*

In the light of the results above, we re-examined the assumption that the motion of the lid produces an approximately uniform shear flow, for both sets of experiments. The Stokes flow in a cylindrical tank of radius $R$ and height $H$, with a rigid lid rotating at angular velocity $\omega$, can be obtained using separation of variables in cylindrical polar coordinates $(\rho, \phi, z)$. The velocity has only an azimuthal component $V$, which is given by

$$V(\rho, z) = \omega R \sum_{n=1}^{\infty} \alpha_n \, \mathrm{J}_1(k_n \rho / R) \, \frac{\sinh(k_n z/R)}{\sinh(k_n H/R)}, \tag{5.5}$$

where

$$\alpha_n = \frac{2}{[\mathrm{J}_0(k_n)]^2} \int_0^1 \xi^2 \mathrm{J}_1(k_n \xi) \, \mathrm{d}\xi = -\frac{2}{k_n \mathrm{J}_0(k_n)}, \tag{5.6}$$

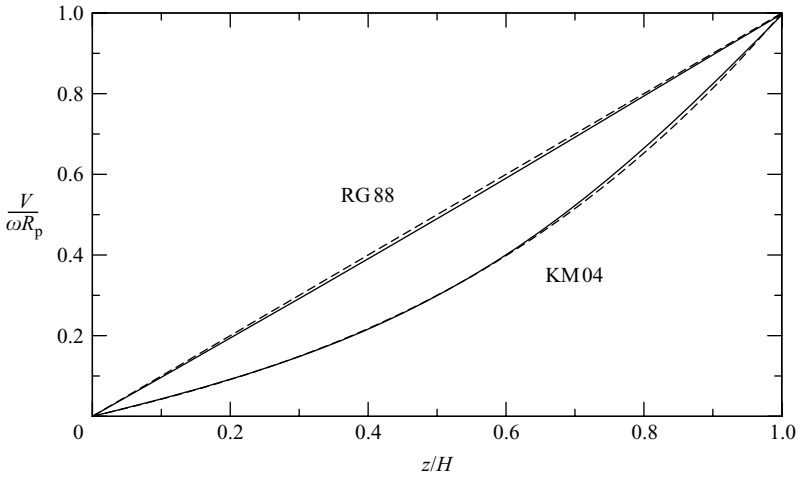


FIGURE 5. Theoretical velocity profiles (solid lines) computed using the expansion (5.5) and evaluated at the radius $R_p$ where the plumes were released. The parameters used for Richards & Griffiths (1988) (RG88) were $R = 30$ cm, $H = 10.5$ cm, $R_p = 12$ cm. Those used for Kerr & Mériaux (2004) (KM04) were $R = 30$ cm, $H = 24$ cm, $R_p = 15$ cm. The dashed lines show approximations to the theoretical solutions: uniform shear for RG88, and the cubic approximation (5.7) for KM04.

and $k_n$ are the positive roots of the Bessel function $J_1$. Each term in the series (5.5) satisfies the zero-velocity conditions on $z = 0$ and $\rho = R$. The coefficients $\alpha_n$ are determined by applying the boundary condition $V(\rho, H) = \omega\rho$.

Calculations of the velocity profiles $V(R_p, z)$ experienced by the plumes in the two sets of experiments are shown in figure 5. The profile for the experiments of Richards & Griffiths (1988) is a very good approximation to uniform shear, as they verified with a dye streak. Hence repeating the numerical calculations with the exact profile would not produce any significant changes to figure 3. However, owing to the larger values of $H/R$ and $R_p/R$, the experiments of Kerr & Mériaux (2004) had a profile that deviated significantly from uniform shear (figure 5). In particular, the velocity near the bottom of the tank is predicted to be less than half that under a uniform-shear assumption.

The numerical computations for Kerr & Mériaux's experiments were therefore repeated with the shear velocity $\gamma z$ (with $\gamma = \omega R_p/H$) replaced, for simplicity, by a cubic polynomial approximation

$$V \approx \gamma z \left[1 - 0.6\left(1 - \frac{z}{H}\right) - 0.4\,\frac{z}{H}\left(1 - \frac{z}{H}\right)\right] \tag{5.7}$$

to (5.5) (see figure 5). Much better agreement was obtained, and the results can be seen in figure 6.

### 5.4. *Discussion of model comparison with experiments*

Considering that the model has no adjustable parameters, the agreement with the experiments, as shown in figures 3 and 6 is quite good in most, but not all, of the runs. We now discuss some of the modelling assumptions and possible reasons for the discrepancies. We note that, with the exception of experiment B1, all the errors in the trajectory predictions are such that the model predicts a greater deflection than is actually observed. There is, however, no systematic variation of the error with deflection angle.

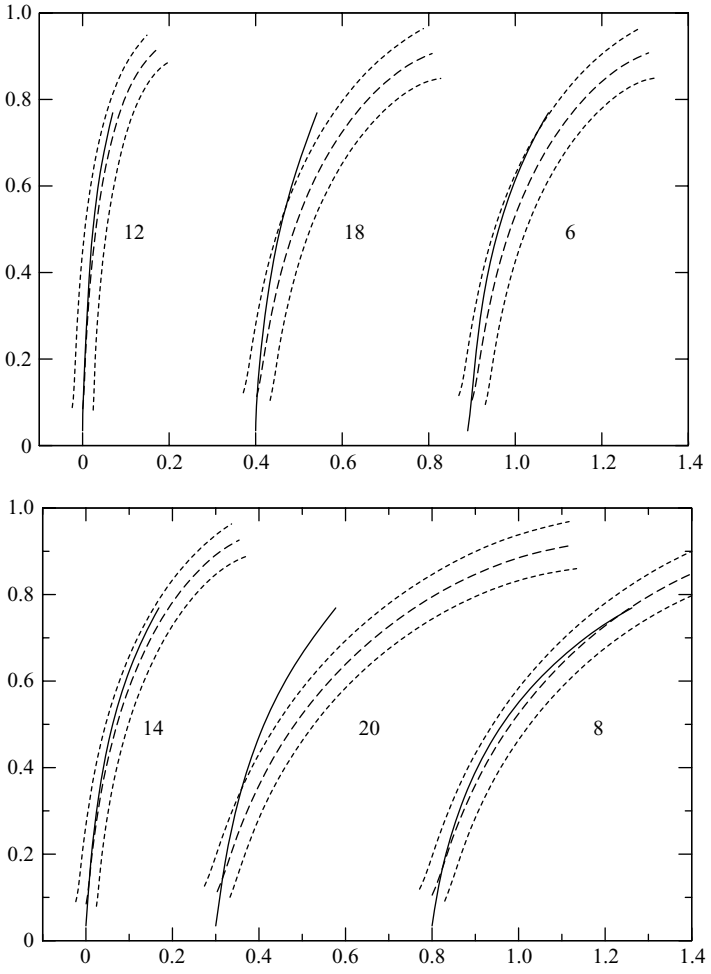


FIGURE 6. A comparison of the model predictions with the experiments of Kerr & Mériaux (2004). The dashed lines are the results (centreline and width at $\pm\sqrt{2}a$) from the model using the non-uniform shear velocity (5.7). Note the significant improvement over figure 4.

One obvious weakness of the model is the requirement for slenderness, and the corrections to slender-body theory that have been neglected. Since $C_2 \approx -1.3$, we need a reasonably large aspect ratio $\ell/a$ even to predict a positive value of $\bar{u}$, let alone reach the regime in which slender-body theory is a good approximation. Since $\ell = z(1 - z/H)$ the maximum value of $\ell$ is only $\frac{1}{4}H$, which exacerbates the difficulty. Taking Richards & Griffiths' experiment A3 as a typical example, the mid-height aspect ratio is about 12, giving a value of only 2.5 for $\ln(\ell/a)$. There is evidence for over-estimation of the deflection of the thicker plumes in figure 3, and some, but not all, of the thicker plumes in figure 6.

The model also implicitly assumes that the plumes remain roughly cylindrical and that non-axisymmetric effects are negligible. Whittaker & Lister (2008) show that for an isolated thermal rising in Stokes flow, much of the buoyant material is stretched out behind in a long tail, rather than remaining in a compact roughly spherical head. If these results carry over to the two-dimensional cross-section of a sheared plume,

then it is plausible (at least for diffusing plumes) that the shear flow in each horizontal cross-section will strip some of the buoyant plume material into a horizontal wake on the downstream side of the plume. However, it seems likely that this effect will serve to increase, rather than decrease, the angle of inclination from that predicted by the model.

The compositional plumes of Richards & Griffiths (1988) had negligible diffusion and thus a constant mass flux. For simplicity, we assumed that the mass flux in the thermal plumes of Kerr & Mériaux (2004) grew according to the diffusive law (3.16) rather than the entrainment mechanism suggested by Griffiths & Campbell (1991). A slow cross-stream circulation was observed in experiments 8 and 20, though it would be surprising if this had led to significant entrainment. In any case, we note that the effect of entrainment would be to increase the plume radius, decrease the rise velocity through the logarithm in (3.20), and thus increase the predicted angle of inclination. Again this is in the opposite direction from that required to make the model agree more closely with experiments.

We also assumed that any viscosity variations are negligible. In fact, in all the experiments considered, the plume material had a lower viscosity than that of the ambient fluid owing either to compositional effects or to temperature-dependent viscosity; viscosity ratios are given in tables 2 and 3. This does not appear to have had a great effect on the results, since there is no obvious correlation between larger viscosity contrasts and larger discrepancies. From a theoretical point of view, viscosity contrasts affect the constants $c_i$, which are quite small (an order of magnitude less than the $C_i$), so a correspondingly large contrast would be required for this change to be significant. A faster axial velocity $\bar{w}$ would result in a smaller buoyancy force $F$ per unit length for a given value of $B$. But it is not the axial velocity that directly controls the angle of inclination. The angle $\theta$ is determined by the transverse velocity $\bar{u}$, which (for a given $F$) will be influenced far less by the lower internal viscosity than $\bar{w}$.† Hence the smaller value of $F$ will dominate the effect of a slightly larger value of $c_2$ in (3.20), thus causing $\bar{u}$ to be smaller. Hence a lower internal viscosity would be expected to cause plumes to be deflected by more than the isoviscous model predicts, which is contrary to the observed discrepancies.

Of the effects discussed above, it appears that departures from asymptotic slenderness are the most likely explanation for the differences between the model and the experiments, though this is far from proven.

## 6. Concluding remarks

We have developed a model for sheared plumes which has some advantages, discussed below, over those proposed before. We have also identified the key dimensionless parameters and regimes for such plumes, along with suitable non-dimensionalizations. This may allow easier comparison between experiments and theory in the future. The dimensionless model is summarized in § 3.4.

The model developed here uses slender-body theory for the plume, which is mathematically more satisfactory than assuming a constant rise velocity. By taking into account the horizontal boundaries, we have also shown how to determine

† Compare with the rise of a uniform buoyant cylinder (see Lister & Kerr 1989, for example). The rise velocity is principally controlled by the outer viscosity, with the viscosity ratio only having a small effect. There is only about a 50% difference between the rise speed of a infinitely viscous rigid cylinder and that of an inviscid cylindrical bubble.

the appropriate aspect ratio. The end result is that the model requires no fitting parameters. It also makes it explicit that the velocity that determines the deflection angle is the transverse induced flow $\bar{u}$, rather than the axial induced flow $\overline{w}$.

The model also has the advantage of relative simplicity. It is probably the best that can be achieved with only local cross-sectionally averaged variables. Any improvements would have to come from incorporating either additional information from the internal buoyancy distribution within the plume, or additional non-local information about the global trajectory and distribution of $F$. If the results here are deemed unsatisfactory, then these complications would need to be incorporated, perhaps even by a full numerical calculation of the three-dimensional Stokes flow and heat transport.

The agreement with experiments (see figures 3 and 6) is by no means perfect, though it is reasonable considering that there are no fitting parameters in the model. The agreement is best for slender plumes, and the model appears to overpredict the deflection of fat plumes. Further work needs to be done to assess the model's performance more fully and to examine more closely where discrepancies arise.

Finally, we note that the applicability of the model is not restricted to steady plumes in uniform shear flows. As we have seen above, it is straightforward to adapt it for use in an arbitrary flow by replacing the occurrences of $\mathscr{G}z$ in (3.19)–(3.23) with an alternative flow field. The model could also be used to predict the temporal evolution of a plume (for example, in response to a change in the external flow) by modifying (3.7) to describe advection of the plume in the direction of its normal. In particular, it would be possible replace the plume rise model of Richards & Griffiths (1988) by the model described here in Steinberger & O'Connell's (1998) calculations of the evolution of mantle plumes in a mantle velocity field inferred from plate motions and tomography.

## Appendix A. Calculations for the outer velocity

In this Appendix, we provide outlines of the calculations behind the results quoted in (3.10)–(3.12) for $\ell$ and $C_i$. Contributions come from the buoyancy throughout the whole of the plume, and include the effects of any boundaries above or below the fluid domain. However, we wish to estimate these parameters using only local properties of the plume.

The parameters $\ell$ and $C_i$ are defined by (3.8) and (3.9) in terms of the outer limit of an inner flow, which must therefore also be the inner limit of an outer flow. As shown in Whittaker & Lister (2006*a*), for plumes whose properties vary only slowly along their length, the outer flow can be represented by a set of Stokeslets on the plume axis. Moreover, it was shown there that the local velocity near the plume at any point is dominated by that of a uniform plume with the corresponding local properties applying throughout. We therefore consider flows driven by a line of Stokeslets of uniform strength.

### A.1. *Straight inclined plume above a single rigid boundary*

First, we consider the velocity induced by a uniform line of Stokeslets at a fixed angle above a single rigid boundary. The length $\ell$ and corrections $C_i$ can be evaluated exactly as functions of $\theta$. We use the method of images described in § 4 of Whittaker & Lister (2006*a*) (see also Pozrikidis 1992, § 3.3) to express the velocity as the integral

$$\boldsymbol{u}(\boldsymbol{x}) = \int_0^\infty F\hat{\boldsymbol{e}}_z \cdot \boldsymbol{K}(\boldsymbol{x}; s')\,\mathrm{d}s'. \tag{A 1}$$

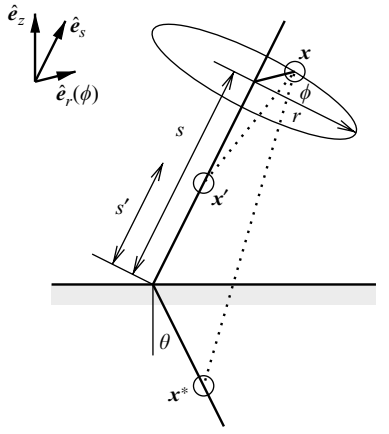


FIGURE 7. The coordinates and points used in the calculation of Appendix A.1. We use a Green's function for the velocity induced at $\boldsymbol{x}$ by a Stokeslet at $\boldsymbol{x}'$. The free-space Green's function is added to that of an appropriate image system at $\boldsymbol{x}^*$, chosen to satisfy the no-slip boundary condition at $z=0$.

The Green's function for the velocity at a point $\boldsymbol{x}$ due to the Stokeslet at $\boldsymbol{x}'$ and image system $\boldsymbol{x}^*$ is

$$\hat{\boldsymbol{e}}_z\cdot\boldsymbol{K} = \left(\frac{\hat{\boldsymbol{e}}_z}{|\boldsymbol{y}'|}+\frac{(\hat{\boldsymbol{e}}_z\cdot\boldsymbol{y}')\boldsymbol{y}'}{|\boldsymbol{y}'|^3}\right)-\left(\frac{\hat{\boldsymbol{e}}_z}{|\boldsymbol{y}^*|}+\frac{(\hat{\boldsymbol{e}}_z\cdot\boldsymbol{y}^*)\boldsymbol{y}^*}{|\boldsymbol{y}^*|^3}\right)$$
$$+2s'\cos\theta\left(\frac{\boldsymbol{y}^*}{|\boldsymbol{y}^*|^3}-\frac{3(\hat{\boldsymbol{e}}_z\cdot\boldsymbol{y}^*)^2\boldsymbol{y}^*}{|\boldsymbol{y}^*|^5}\right)-2s'^2\cos^2\theta\left(\frac{\hat{\boldsymbol{e}}_z}{|\boldsymbol{y}^*|^3}-\frac{3(\hat{\boldsymbol{e}}_z\cdot\boldsymbol{y}^*)\boldsymbol{y}^*}{|\boldsymbol{y}^*|^5}\right), \quad (A\,2)$$

where, using the notation of figure 7,

$$\boldsymbol{y}' \equiv \boldsymbol{x}-\boldsymbol{x}' = (s-s')\hat{\boldsymbol{e}}_s + r\hat{\boldsymbol{e}}_r, \quad (A\,3)$$
$$\boldsymbol{y}^* \equiv \boldsymbol{x}-\boldsymbol{x}^* = (s-s')\hat{\boldsymbol{e}}_s + 2s'\cos\theta\,\hat{\boldsymbol{e}}_z + r\hat{\boldsymbol{e}}_r. \quad (A\,4)$$

We were unable to evaluate the full integral (A 1) analytically. However, we are only interested in the limiting behaviour of the velocity close to the plume. There is a logarithmic singularity from the first two terms in (A 2) and the remaining terms only contribute to the constant and higher-order terms. We also note that the velocity is proportional to $F$ and a function only of $r/s$ and $\phi$, so we can set $s=F=1$ without loss of generality.

We consider a second kernel

$$\widetilde{\boldsymbol{K}} = \begin{cases} \left(\dfrac{\boldsymbol{I}}{|\boldsymbol{y}'|}+\dfrac{\boldsymbol{y}'\boldsymbol{y}'}{|\boldsymbol{y}'|^3}\right) & : \quad 0<s'<2 \\ \boldsymbol{0} & : \quad \text{otherwise}, \end{cases} \quad (A\,5)$$

which has a known integral and has the same singular behaviour as $\boldsymbol{K}$ near $r=0$. We are then able to evaluate

$$\int_0^\infty \hat{\boldsymbol{e}}_z\cdot(\boldsymbol{K}-\widetilde{\boldsymbol{K}})\,\mathrm{d}s' \quad (A\,6)$$

analytically at $r=0$. By adding the constant term and logarithmic behaviour due to $\widetilde{\boldsymbol{K}}$ to this result, we obtain the logarithmic and $O(1)$ behaviour of the full outer velocity as $r/s\to 0$. Comparing with (3.8) and (3.9), we see that this is precisely what

is required to evaluate $\ell$ and the $C_i$. Taking $\ell = z$ for simplicity, the results for the $C_i$ are given in (3.11) and (3.12).

Since the velocities are dominated by contributions from the local buoyancy, and in the absence of a better analytical result, we shall apply these results for a line of Stokeslets to calculations for plumes with varying inclination $\theta(s)$ by evaluating them with the local value of $\theta$ at each point.

### A.2. *Vertical plume between two free-slip boundaries*

Secondly, we calculated the equivalent results for a vertical plume between two free-slip boundaries at $z = 0$ and $z = 1$. (Both the rigid case and the case $\theta \neq 0$ appear to be intractable.)

The vertical velocity induced at a point $(s, z)$ in an unbounded domain by an isolated Stokeslet of strength $\hat{\boldsymbol{e}}_z$ at $(0, z')$ is given by

$$J(s, z; z') = \frac{s^2 + 2(z - z')^2}{[s^2 + (z - z')^2]^{3/2}}\,. \tag{A 7}$$

We now consider the total velocity $w(s, z)$ as an integral over a line of such Stokeslets for $0 < z' < 1$ together with the appropriate images for $z' < 0$ and $z' > 1$. For free-slip boundaries the images are simply Stokeslets of the same strength reflected in the boundaries. These reflections result in a Stokeslet density along the axis which is of uniform magnitude but which reverses direction at unit intervals.

Defining

$$I_n(s, z) = \int_n^\infty \{J(s, z; z') - J(s, z; -z')\}\,\mathrm{d}z', \tag{A 8}$$

the velocity is given by

$$\begin{aligned} w(s, z) &= (I_0 - I_1) - (I_1 - I_2) + (I_2 - I_3) - (I_3 - I_4) + \cdots \\ &= I_0(s, z) + 2\sum_{n=1}^{\infty} (-1)^n\, I_n(s, z). \end{aligned} \tag{A 9}$$

The integrals $I_n$ can be evaluated explicitly, but all we actually need is the limiting behaviour as $s/z \to 0$. We find that

$$I_0(s, z) = -4 \ln\left(\frac{s}{z}\right) + 4 \ln 2 - 2 + O\left(\frac{s}{z}\right), \tag{A 10}$$

$$I_n(s, z) = 2 \ln\left(\frac{n + z}{n - z}\right) + O\left(\frac{s}{z}\right) \quad (n \geqslant 1). \tag{A 11}$$

Evaluating the sum (A 9) with the help of formula 8.325(1) in Gradshteyn & Ryzhik (2000), we find that

$$w(s, z) = -4 \ln\left(\frac{s}{\mathscr{L}}\right) + 4 \ln 2 - 2 + O\left(\frac{s}{z}\right) \tag{A 12}$$

where

$$\mathscr{L} = \frac{2\Gamma\left(1 - \frac{1}{2}z\right)\Gamma\left(1 - \frac{1}{2}(1 - z)\right)}{\Gamma\left(\frac{1}{2}z\right)\Gamma\left(\frac{1}{2}(1 - z)\right)}. \tag{A 13}$$

Comparing $w(s, z)$ with $I_0(s, z)$, which is in fact the corresponding result for a single lower boundary, we identify $\mathscr{L}$ with the appropriate outer length $\ell$. To within an

accuracy of 8%, (A 13) may be approximated by

$$\ell = z(1-z). \tag{A 14}$$

Since $\ell$ only appears in the model in a logarithm, this is a sufficiently good approximation. We shall assume that the simplified expression (A 14) is also appropriate for sheared plumes between two rigid horizontal boundaries, with the values of $C_i$ obtained above.

## Appendix B. Calculations for the inner velocity

In this Appendix, we outline the calculations of the constants $c_i$ for some specific buoyancy distributions as discussed in § 3.2. For a slender plume, the length scale of variation along the axis is large compared with the width $a$. For $r/a \leqslant O(1)$, the Stokes equations (2.1) and (2.2) can be simplified by neglecting axial derivatives. By matching to the far-field behaviour (3.8) and (3.9), we can obtain an explicit solution for the flow field inside the plume induced by a given buoyancy distribution. This is then used to determine $c_1$ and $c_2$.

With the non-dimensionalization used in the model, the Stokes equations simplify and decouple to

$$\nabla_\perp^2 w = -2\pi b \cos\theta, \tag{B 1}$$

$$\nabla_\perp^2 \boldsymbol{u}_\perp = \nabla_\perp p - 2\pi b \sin\theta\, \hat{\boldsymbol{e}}_t, \qquad \nabla_\perp \cdot \boldsymbol{u}_\perp = 0, \tag{B 2}$$

where the subscript $\perp$ denotes components in the local $(r,\theta)$-plane, and $\hat{\boldsymbol{e}}_t$ is the unit vector in the $r$-direction when $\phi = \pi$. The far-field boundary conditions are given by (3.8) and (3.9) in terms of the $C_i$.

It is convenient to use a horizontal coordinate $\xi = r/a$, to rescale the buoyancy as

$$b(r) = \frac{F}{a^2}\tilde{b}(\xi), \tag{B 3}$$

and to write the inner velocity in the form

$$w = F\cos\theta \left\{ \ln\left(\frac{\ell}{a}\right) + C_1 + f_1(\xi,\phi) \right\}, \tag{B 4}$$

$$u = \frac{F\sin\theta}{2} \left\{ \ln\left(\frac{\ell}{a}\right) + C_2 + \left(\cos^2\phi - \tfrac{1}{2}\right) + f_2(\xi,\phi) \right\}. \tag{B 5}$$

The far-field boundary condition is then $f_i(\xi,\phi) \sim -\ln\xi + o(1)$ as $\xi \to \infty$.

We now calculate the velocities $f_i(\xi,\phi)$ in terms of the scaled buoyancy $\tilde{b}(\xi)$, by using a Green's function. We write

$$f_i(\xi,\phi) = 2\pi \int_0^\infty G_i(\xi,\phi;\xi')\,\tilde{b}(\xi')\,\xi'\,\mathrm{d}\xi'. \tag{B 6}$$

For the axial velocity

$$G_1(\xi,\phi;\xi') = \begin{cases} -\ln\xi' & : \quad 0 < \xi < \xi' \\ -\ln\xi & : \quad \xi' < \xi < \infty, \end{cases} \tag{B 7}$$

which is easily obtained from (B 1). For the transverse velocity,

$$G_2(\xi,\phi;\xi') = \begin{cases} -\ln\xi' - \left(\cos^2\phi - \tfrac{1}{2}\right) & : \quad 0 < \xi < \xi' \\ -\ln\xi - \left(\cos^2\phi - \tfrac{1}{2}\right)\dfrac{\xi'^2}{\xi^2} & : \quad \xi' < \xi < \infty, \end{cases} \tag{B 8}$$

which can be derived from (B 2) using, for example, Papkovich–Neuber potentials.

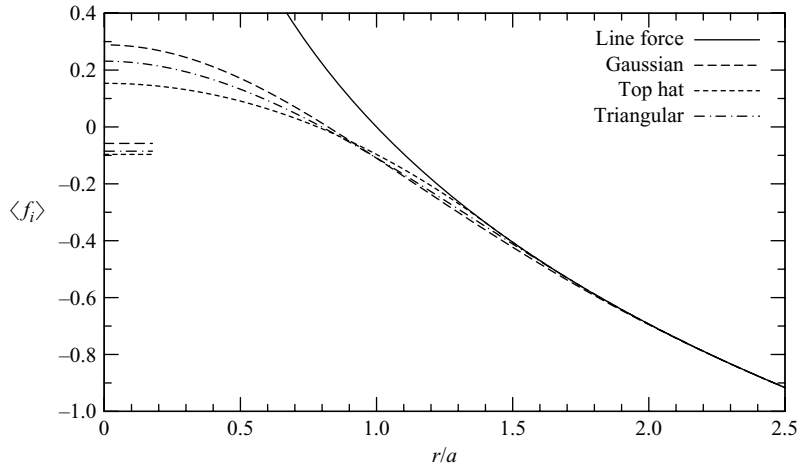


FIGURE 8. The velocity driven by the axisymmetric buoyancy distributions (B 10). The function plotted is the axisymmetric component of $f_i$ from (B 4) and (B 5), which is the same for both the axial and transverse velocities. The short horizontal segments by the left-hand axis indicate the corresponding values of $c_i$ as given by (B 11).

Once the velocity is obtained, application of (3.3) and (3.4), and comparison with (3.13) and (3.14), gives

$$c_i = \int_0^{2\pi}\int_0^{\infty} \tilde{b}(\xi)\, f_i(\xi,\phi)\, \xi \, \mathrm{d}\xi \, \mathrm{d}\phi. \tag{B 9}$$

Results are computed for the three simple axisymmetric buoyancy distributions

$$\tilde{b}(\xi) = \begin{cases} \dfrac{1}{\pi}\exp(-\xi^2) & : \text{Gaussian} \\ \dfrac{1}{2\pi}\mathrm{H}(\sqrt{2}-\xi) & : \text{top hat} \\ \dfrac{9}{10\pi}\left(1-\sqrt{3/10}\,\xi\right)\mathrm{H}(\sqrt{10/3}-\xi) & : \text{triangular,} \end{cases} \tag{B 10}$$

where $\mathrm{H}(x)$ is the Heaviside step function, and the amplitude and width of the distributions have been chosen to satisfy (3.1) and (3.2). The resultant velocities are shown in figure 8, and the corresponding values of $c_i$ are

$$c_1 = c_2 = \begin{cases} -\frac{1}{2}(\ln 2 - \gamma) = -0.0581 & : \text{Gaussian} \\ -\frac{1}{2}\left(\ln 2 - \frac{1}{2}\right) = -0.0966 & : \text{top hat} \\ -\frac{1}{2}\left(\ln \frac{10}{3} - \frac{31}{30}\right) = -0.0853 & : \text{triangular.} \end{cases} \tag{B 11}$$

The smallness of the corrections $c_i$ and their insensitivity to the buoyancy distribution mean that, even at modest aspect ratios, the effects of the internal buoyancy distribution can be neglected with little loss in accuracy. We anticipate that non-axisymmetric perturbations to the buoyancy distribution will not have a significant effect on these results.

## REFERENCES


Albers, M. & Christensen, U. R. 1996 The temperature excess of plumes rising from the core–mantle boundary. *Geophys. Res. Lett.* **23**, 3567–3570.

Batchelor, G. K. 1970 Slender-body theory for particles of arbitrary cross-section in Stokes flow. *J. Fluid Mech.* **44**, 419–440.

Cox, R. G. 1970 The motion of long slender bodies in a viscous fluid. Part 1. General theory. *J. Fluid Mech.* **44**, 791–810.

Davaille, A., Girard, F. & Le Bars, M. 2002 How to anchor hot spots in a convecting mantle. *Earth Planet. Sci. Lett.* **203**, 621–634.

Gradshteyn, I. S. & Ryzhik, I. M. 2000 *Table of Integrals Series and Products*, 6th edn. Academic.

Griffiths, R. W. & Campbell, I. H. 1991 On the dynamics of long-lived plume conduits in the convecting mantle. *Earth Planet. Sci. Lett.* **103**, 214–227.

Hinch, E. J. 1991 *Perturbation Methods*. Cambridge University Press.

Jellinek, M. & Manga, M. 2002 The influence of a chemical boundary layer on the fixity, spacing and lifetime of mantle plumes. *Nature* **418**, 760–763.

Jellinek, M. & Manga, M. 2004 Links between long-lived hot spots, mantle plumes, D″, and plate tectonics. *Rev. Geophys.* **42**, RG3002.

Keller, J. B. & Rubinow, S. I. 1976 Slender-body theory for slow viscous flow. *J. Fluid Mech.* **75**, 705–714.

Kerr, R. C. & Lister, J. R. 1988 Island arc and mid-ocean ridge volcanism, modelled by diapirism from linear source regions. *Earth Planet. Sci. Lett.* **88**, 143–152.

Kerr, R. C. & Mériaux, C. 2004 Structure and dynamics of sheared mantle plumes. *Geochem. Geophys. Geosyst.* **5**, Q12009.

Lister, J. R. & Kerr, R. C. 1989 The effect of geometry on the gravitational instability of a buoyant region or viscous fluid. *J. Fluid Mech.* **202**, 577–594.

Loper, D. E. & Stacey, F. D. 1983 The dynamical and thermal structure of deep mantle plumes. *Phys. Earth Planet. Inter.* **33**, 304–317.

Molnar, P. & Atwater, T. 1973 Relative motion of hot spots in the mantle. *Nature* **246**, 288–291.

Molnar, P. & Stock, J. 1987 Relative motions of hotspots in the Pacific, Atlantic and Indian Oceans since late cretaceous time. *Nature* **327**, 587–591.

Morgan, W. J. 1971 Convection plumes in the lower mantle. *Nature* **230**, 42–43.

Morgan, W. J. 1972 Plate motions and deep mantle convection. *Mem. Geol. Soc. Am.* **132**, 7–22.

Olson, P., Schubert, G. & Anderson, C. 1993 Structure of axisymmetric mantle plumes. *J. Geophys. Res.* **98** (B4), 6829–6844.

Olson, P. & Singer, H. 1985 Creeping plumes. *J. Fluid Mech.* **158**, 511–531.

Pozrikidis, C. 1992 *Boundary Integral and Singularity Methods for Linearized Viscous Flow*. Cambridge University Press.

Richards, M. A. & Griffiths, R. W. 1988 Deflection of plumes by mantle shear flow: Experimental results and a simple theory. *Geophys. J.* **94**, 367–376.

Richards, M. A. & Griffiths, R. W. 1989 Thermal entrainment by deflected mantle plumes. *Nature* **342**, 900–902.

Skilbeck, J. N. & Whitehead, Jr., J. A. 1978 Formation of discrete islands in linear island chains. *Nature* **272**, 499–501.

Stacey, F. D. & Loper, D. E. 1983 The thermal boundary-layer interpretation of D″ and its role as a plume source. *Phys. Earth Planet. Inter.* **33**, 45–55.

Steinberger, B. 2000 Plumes in a convecting mantle: Models and observations for individual hotspots. *J. Geophys. Res.* **105** (B5), 11127–11152.

Steinberger, B. & O'Connell, R. J. 1998 Advection of plumes in mantle flow: Implications for hotspot motion, mantle viscosity and plume distribution. *Geophys. J. Intl* **132**, 412–434.

Turner, J. S. 1973 *Buoyancy Effects in Fluids*. Cambridge University Press.

Whitehead, J. A. 1982 Instabilities of fluid conduits in a flowing Earth – are plates lubricated by the asthenosphere? *Geophys. J. R. Astron. Soc.* **70**, 415–433.

Whitehead, J. A. 1988 Fluid models of geological hotspots. *Annu. Rev. Fluid Mech.* **20**, 61–87.

Whittaker, R. J. & Lister, J. R. 2006*a* Steady axisymmetric creeping plumes above a planar boundary. Part 1. A point source. *J. Fluid Mech.* **567**, 361–378.

Whittaker, R. J. & Lister, J. R. 2006*b* Steady axisymmetric creeping plumes above a planar boundary. Part 2. A distributed source. *J. Fluid Mech.* **567**, 379–397.

Whittaker, R. J. & Lister, J. R. 2008 The self-similar rise of a buoyant thermal in very viscous flow. *J. Fluid Mech.* **606**, 295–324.

Wilson, J. T. 1965 Evidence from ocean islands suggesting movement in the Earth. *Phil. Trans. R. Soc. Lond.* A **258**, 145–167.

Yuen, D. A. & Schubert, G. 1976 Mantle plumes: A boundary layer approach for Newtonian and non-Newtonian rheologies. *J. Geophys. Res.* **81**, 2499–2510.